Experimental Determination of the Electron Density Topology in a Non-centrosymmetric Transition Metal Complex: $[Ni(H_3L)][NO_3][PF_6]$ [H_3L = *N*,*N*′,*N*″-Tris(2-hydroxy-3-methylbutyl)-1,4,7-triazacyclononane]

G. T. Smith,[†] P. R. Mallinson,*[,‡] C. S. Frampton,[‡,§] L. J. Farrugia,[‡] R. D. Peacock,[‡] and J. A. K. Howard[†]

Contribution from the Departments of Chemistry, University of Durham, Durham DH1 3LE, England, and University of Glasgow, Glasgow G12 8QQ, Scotland

Received December 11, 1996. Revised Manuscript Received March 24, 1997[⊗]

Abstract: We have determined the experimental charge density of the title compound, a large pendant arm macrocyclic complex, by fitting a multipole model to high-resolution X-ray diffraction data. We find redistribution of the charge density from the ligating nitrogen and oxygen atoms to the central nickel ion which considerably reduces the charge on the metal. While the d-orbital populations are in agreement with ligand-field theory, the charge density of the metal shows diffuse features which are ascribed to metal 4s and 4p participation in the metal−ligand bonding. Additionally, the trigonal-planar arrangement of critical points in $-\nabla^2\rho(\mathbf{r})$ within the valence shell charge concentration (VSCC) of the ligating oxygen atom provides evidence for metal−oxygen π-bonding.

Introduction

The ability of current computational procedures to produce wave functions of extremely high accuracy including correlation effects is a triumph of contemporary quantum chemistry and has led to many great insights into chemical bonding, reaction pathways, and dynamical and spectroscopic processes.[1−11] However, the standard ab-initio procedures rapidly become unmanageable with increasing size of the system under study.[12] One way of overcoming this problem is to treat only valence electrons and model the effect of the atomic core by a pseudopotential.[13] A relatively recent addition to the quantum chemist's armory has been density functional theory (DFT),[14] which promises an approximate treatment of electron correlation effects with a computational cost of the same magnitude as Hartree−Fock level calculations, and the application of this methodology to important chemical problems continues apace.[15−17] There still exists an upper limit to the size of the system which can be studied by this method.

A feasible alternative for the study of structure and bonding in large molecules is the determination of the electron density by fitting high-resolution single-crystal X-ray diffraction data to a multipole model which explicitly accounts for the complicated nature of the valence density.[18] In fact, in his timeless text on transition metal complexes,[19] Orgel mused on the insight which would be provided by such a technique before the technical difficulties inherent in the method had been overcome. An immediate advantage of this approach is that the charge density obtained is by definition correlated, being a representation of the true density. This density may be analyzed subsequently using Bader's Theory of Atoms in Molecules.[20,21] The results presented in this work use exactly these techniques to investigate the fundamental nature of metal−ligand bonding in a large N-substituted triaza macrocycle. This molecule is sufficiently large and of low enough symmetry to lie on the upper limits of what can be tackled by theoretical techniques and provides important independent results with which to compare any such theoretical calculations. We also believe this to be the most difficult experimental determination of the topological properties of the charge density attempted so far due to the size of the complex and the non-centrosymmetric space group of the crystal.

The particular macrocyclic complex chosen, $[Ni(H_3L)]^{2+}$-$[NO_3]^-[PF_6]^-$ [H_3L = *N*,*N*′,*N*″-tris(2-hydroxy-3-methylbutyl)-1,4,7-triazacyclononane] (**1**), is of interest because the metal atom is ligated by tertiary amine nitrogen atoms and alcohol oxygen atoms. The former is conventionally thought of as a

[†] University of Durham.
[‡] University of Glasgow.
[§] Present address: Roche Products Ltd. P.O. Box 8, Welwyn Garden City, Herts AL7 3AY, England.
[⊗] Abstract published in *Advance ACS Abstracts,* May 1, 1997.

(1) Simons, J.; Gutowski, M. *Chem. Rev.* **1991**, *91*, 669−677.
(2) Clementi, E.; Corongin, G.; Bahattacharya, D.; Feuston, B.; Frye, D.; Preiskorn, A.; Rizzo, A.; Xue, W. *Chem. Rev.* **1991**, *91*, 679−699.
(3) Bauschlicher, W. J., Jr.; Langhoff, S. R. *Chem. Rev.* **1991**, *91*, 701−718.
(4) Pepper, M.; Bursten, B. E. *Chem. Rev.* **1991**, *91*, 719−741.
(5) Newton, M. D. *Chem. Rev.* **1991**, *91*, 767−792.
(6) Pullman, A. *Chem. Rev.* **1991**, *91*, 793−812.
(7) Cory, M. G. *Chem. Rev.* **1991**, *91*, 813−822.
(8) Koga, N.; Morokuma, K. *Chem. Rev.* **1991**, *91*, 823−842.
(9) Orlandi, G.; Zerbetto, F.; Zgierski M. Z. *Chem. Rev.* **1991**, *91*, 867−891.
(10) Canadell, E.; Whangbo, M.-H. *Chem. Rev.* **1991**, *91*, 965−1034.
(11) Bonačić, V.; Fantucci, P.; Kontecký, J. *Chem. Rev.* **1991**, *91*, 1035−1108.
(12) Veillard, A. *Chem. Rev.* **1991**, *91*, 743−766.
(13) Szasz, L. *Pseudopotential Theory of Atoms and Molecules*; Wiley: New York, 1985.
(14) Parr, R. G.; Yang, W. *Density-Functional Theory of Atoms in Molecules*; Oxford University Press: New York, 1989.
(15) Labonowski, J. K.; Andzelm, J. W. *Density-Functional Methods in Chemistry*; Springer-Verlag: New York, 1991.
(16) Ziegler, T. *Chem. Rev.* **1991**, *91*, 651−667.
(17) Kohn, W.; Becke, A. D.; Parr, R. G. *J. Phys. Chem.* **1996**, *100*, 12974−12980.
(18) Hansen, N. K.; Coppens, P. *Acta Crystallogr., Sect. A* **1978**, *34*, 909−921.
(19) Orgel, L. E. *An Introduction to Transition-Metal Chemistry, Ligand Field Theory*; Methuen: London, 1960.
(20) Bader, R. F. W. Atoms in Molecules: A Quantum Theory; Oxford University Press: Oxford, U.K., 1990.
(21) Bader, R. F. W. *Chem. Rev.* **1991**, *91*, 893−928.

S0002-7863(96)04264-3 CCC: $14.00

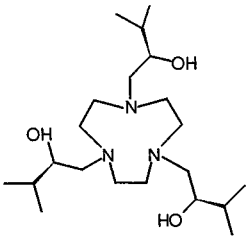

H_3L

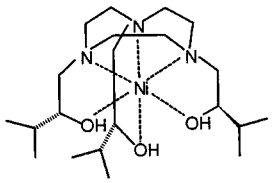

$Ni^{II}H_3L$

very strong σ-donor, while the latter is considered as much weaker in this respect, although potentially capable of π-bonding.

The large difference of the ligating properties of these two atoms should be reflected by the properties of the charge distribution. Additionally, the complex has the low-symmetry point group C_3 in the crystal which is much less studied than the O_h or D_3 cases. The C_3 symmetry and the strong trigonal perturbation are reflected in both the electronic absorption and CD spectra.[22] The electronic spectrum is much more intense ($\epsilon = 13-40$ dm^3 mol cm^{-1}) than that of a typical D_3 tris-chelate such as $[Ni(en)_3]^{2+}$ ($\epsilon = 2-9$ dm^3 mol cm^{-1}). The CD spectrum is even more indicative of strong trigonal mixing. The dissymetry factors for the magnetic dipole allowed transition, and the magnetic dipole forbidden transitions are comparable. This is in contrast to D_3 tris-chelates where the magnetic dipole forbidden transitions have dissymmetry factors 1 order of magnitude weaker than the magnetic dipole allowed transition.

The crystal structure and absolute configuration are as determined previously.[22] Figure 1 shows a thermal ellipsoid plot of the complex cation at the 90% probability level. The nickel ion lies on a crystallographic 3-fold axis and is complexed by three nitrogen atoms above and three oxygen atoms below the basal plane, with an 18° twist away from pseudo-octahedral coordination. The Ni−N and Ni−O bond lengths at 2.064(1) and 2.094(1) Å, respectively, do not indicate a priori any substantial difference in bond characteristics. A preliminary account, using a less flexible model of the charge density has already appeared.[23]

Experimental Section

A dark blue octahedral crystal of **1** was chosen for analysis. High-resolution, single-crystal X-ray diffraction data were measured at 123(1) K on an Enraf-Nonius CAD4 automated diffractometer as previously described.[24] Data reduction was performed with the DREAM[25] program suite, including an analytical absorption correction by Gaussian quadrature using ABSORB.[26] The intensities of five standard reflections were measured every 2 h and fitted to cubic polynomials to scale the data for decay correction, and the instrument instability factor, P, was obtained from the errors in the fit of the polynomials and fluctuations in the standards as described in ref 25. Experimental data are summarized in Table 1.

Multipole Refinements: Background. The multipole refinements were performed using the least-squares module of the XD package.[27] The function $\sum w(|F_o| - k|F_c|)^2$ was minimized where F_o and F_c are the observed and calculated structure factors, respectively, and k is the scale factor which minimizes the sum. Only those reflections with $I > 2\sigma(I)$ were included in the refinement.

The static charge density is described as a sum of rigid pseudoatoms[28] at the nuclear positions ($\mathbf{R}_j$)

$$\rho(\mathbf{r}) = \sum_j \rho_j(\mathbf{r} - \mathbf{R}_j)$$

Each pseudoatom density is expanded in multipolar form[18]

$$\rho_j(\mathbf{r}_j) = P_c\rho_c(\mathbf{r}_j) + \kappa'^3 P_v\rho_v(\kappa'^3\mathbf{r}_j) + \sum_{l=0}^{l_{max}} \sum_{m=-l}^{m=+l} \kappa''^3 P_{lm} R_l(\kappa''\mathbf{r}_j) d_{lmp}(\theta_j, \phi_j)$$

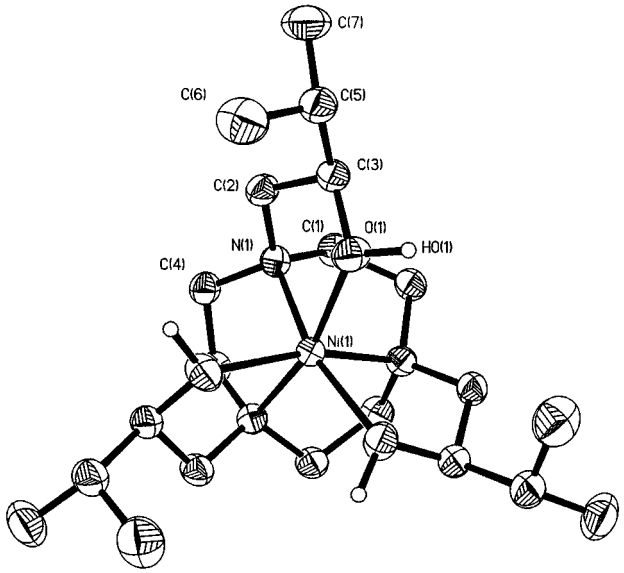

Figure 1. Thermal ellipsoid plot of NiH_3L at the 90% probability level, showing the atomic labels.

Table 1. Experimental Data for $[Ni(H_3L)]^{2+}[NO_3]^-[PF_6]^-$ (**1**)

formula	$[C_{21}H_{45}N_3O_3Ni]^{2+}[NO_3]^-[PF_6]^-$
MW	653.28
crystal system	cubic
space group	$P2_13$
T/K	123(1)
a/Å	14.008(2)
V/Å^3	2748.7(7)
Z	4
D_c/g cm^{-3}	1.578
crystal dimensions/mm	0.4 × 0.4 × 0.6
μ/cm^{-1}	8.47
range of corrections for absorption	0.774−0.804
isotropic extinction	Gaussian mosaic spread 11s (domain size 3.8×10^{-5} cm)
radiation(λ/Å)	Mo Kα (0.7107)
scan type	$\theta-2\theta$
$(\sin\theta/\lambda)_{max}$/Å^{-1}	1.08
standard reflections	8 8 $\bar{8}$, 0 4 9, 0 4 $\bar{9}$, 0 26 0, 4 0 4
no. of reflections measured	20445
range hkl	1−30; 0−30; −17−10
no. of symmetry-independent reflections	6017
no. of $I > 2\sigma(I)$ reflections	5094
agreement factor $R = \sum\|I - I\|/\sum I$	0.017
refined on	F
R	0.0220
R_w	0.0155
S	1.07
no. of variables	400
weighting scheme, w	$w = 1/\sigma^2(F) = 4F^2/\sigma^2(F^2)$ $\sigma^2(F^2) = \sigma^2_{counting}(F^2) + P^2F^4$
P	0.018

(22) Fallis, I. A.; Farrugia, L. J.; Macdonald, N. M.; Peacock, R. D. *J. Chem. Soc., Dalton Trans.* **1993**, 2759−2763.

(23) Smith, G. T.; Mallinson, P. R.; Peacock, R. D.; Farrugia, L. J.; Fallis, I. A.; Frampton, C. S.; Howard J. A. K. *J. Chem. Soc., Chem Commun.* **1996**, 525−526.

(24) Howard, S. T.; Hursthouse, M. B.; Lehmann, C. W.; Mallinson, P. R.; Frampton, C. S. *J. Chem. Phys.* **1992**, *97*, 5616−5630.

(25) Blessing, R. H. *Crystallogr. Rev.* **1987**, *1*, 3.

(26) DeTitta, G. Program ABSORB, Medical Foundation of Buffalo, NY, 1984.

(27) Koritsanszky, T.; Howard, S. T.; Mallinson, P. R.; Su, Z.; Richter, T.; Hansen, N. K. XD − a computer program package for multipole refinement and analysis of charge densities from diffraction data, 1995.

(28) Stewart, R. F. *Acta Crystallogr., Sect. A* **1976**, *32*, 565−574.

where $\mathbf{r}_j = \mathbf{r} - \mathbf{R}_j$. In the present model each atom is described by a frozen core of form ρ_c with a fixed population, and spherical valence of the form ρ_v, with the population; P_v varied in the least-squares procedure to allow charge transfer between atoms. The κ' variable scales the radial exponent, allowing for contraction or expansion of the charge cloud of the pseudoatom. Both ρ_c and ρ_v are derived from Clementi's Hartree−Fock wave functions[29] (we have used the Ni^{2+} scattering factor in this study rather than the neutral one). The final term in the expansion describes the deviation from sphericity of the valence density by a set of deformation functions taking the shape of density normalized spherical harmonics d_{lmp}. The $l = 0$ deformation function, which is a second monopole, is often left out of the refinement. The radial term for these functions may be a simple Slater-type function $R_l(\mathbf{r}) = Nr^n \exp(-\kappa''\zeta\mathbf{r})$ or the relevant order Fourier−Bessel transform of the Clementi Hartree−Fock (HF) wave function. The expansion−contraction coefficient κ'' is again available to improve the radial dependence of the fit. Due to the crystallographic C_3 site symmetry of the Ni atom and counterion N and P atoms, only certain deformation functions may take non-zero populations for these sites.[30] Each non-hydrogen atom has anisotropic displacement parameters (ADPs) refined while the isotropic displacement parameters for the hydrogen atoms were obtained from a preliminary spherical atom refinement of coordinates and displacement parameters for all atoms, using the contracted scattering factor of Stewart Davidson and Simpson[31] for the hydrogen atoms. The C−H bond vectors were then renormalised to 1.06 Å, an average value obtained from neutron diffraction experiments,[32] by adjusting the hydrogen atom coordinates. H(O1) was similarly treated with the O−H bond vector renormalized to 1.00 Å. The hydrogen atom structural parameters were not further refined. An independent measurement of structural parameters could, in principle, be obtained from a parallel neutron diffraction study. However, it is an observation that displacement parameters from such parallel studies may require empirical adjustment for different factors affecting the two types of experiment.[33]

Hydrogen κ' and κ'' were fixed at 1.20 during the multipole refinements, which is equivalent to using the contracted scattering factors.

Application to 1. In all refinements in this study, the charge of each of the counterions was constrained to be −1 and the metal−ligand complex total charge was held at 2+. For the counterions, the κ'' parameters were not refined. The non-centrosymmetric space group $P2_13$, introduces additional complications to multipole refinement resulting from the ambiguity in phase assignment of the reflections. An excellent analysis of this problem has been published recently by El Haouzi et al.[34] In such cases, extreme care must be taken to ensure that the final model is physically sensible and this is best done by examining physical attributes such as the ADPs using Hirshfeld's rigid bond test,[35,36] topological properties, etc. A second complication arises because the multipole model, being a one-centered expansion, is not designed for the efficient projection of diffuse, two centered (or overlap) terms of the experimental density into the model.[37] Here, we specifically mean those parts of the density in the N−Ni and O−Ni bonds, which are far from either nucleus. For example, the 4s and 4p orbitals on the metal which have maximal overlap with the ligand lone pairs are so diffuse that they will contribute only to the very lowest angle data and these data are those most affected by extinction effects.

For organic molecules containing only first-row atoms, many fine multipole studies have been published using the standard multipole model.[38] In our particular case, the standard scattering formalism including expansion to hexadecapolar functions on P and Ni produced a good fit to the data in terms of agreement indices and a reasonable residual map, but resulted in an unconverged κ'' refinement for the ligating N and O atoms which thus became extremely diffuse. One imagines this was due to the functions on these atoms "reaching out" toward the metal to incorporate the density in the metal−ligand bond which is not explicitly accounted for by the model.

Inclusion of hexadecapoles on the ligating atoms caused excessive correlations between these functions and the metal-based multipoles, and the refinement converged with unrealistically high esd for these functions.

It has been shown previously[39−41] that the electron density distribution of the 3d-orbitals of a transition metal can be described fully by the set of multipolar functions of orders 0, 2, and 4. We therefore tried using only these functions in the scattering expression for the nickel atom. While the refinement was stable and converged, the ligating atoms again had unrealistic κ'' values and the C−N, C−O, and metal-to-ligand bonds failed the rigid bond test, indicating deficiencies in the charge density model for the ligating atoms. Additionally, no metal-to-ligand bond paths could be traced in the charge density. It became apparent that it was essential to include the odd-order multipoles on the metal atom which account for valence density other than 3d such as 4s, 4p, and metal−ligand overlap density. This also meant than any analysis based only on metal d-orbital occupancies would be of limited value in describing the metal−ligand bonding. Since the odd-order terms would be describing density which was more diffuse than the 3d density, we reasoned that a more elaborate radial treatment of the metal would be appropriate. Thus 3d HF radial functions were assigned to the first monopole and to the order 2 and 4 multipoles. A Slater-type radial function was assigned to the 0, 1, and 3 order multipoles. We refined individual κ parameters for these three sets, and an acceptable, stable refinement resulted. The C−N and C−O bonds became acceptable in terms of the rigid bond test, indicating that physically sensible ADPs for the ligating atoms and bond paths with (3, −1) critical points were located between the metal and ligating atoms. However, the N−Ni and O−Ni bonds still failed the rigid bond test, having values of 0.0015 and 0.0018 $Å^2$, respectively, compared to the Hirshfeld criterion of ≤ 0.001 $Å^2$. This could indicate that the metal ADPs are deficient in some way, or may just be a reflection of the substantial difference in mass between these bonded atoms. The κ value for the HF monopole took the value of 1.04(1), while the order 2 and 4 κ was 1.15(4). Both of these are slightly contracted compared with the free metal ion. The κ value of the 0, 1, and 3 order multipoles with the Slater-type radial function (which were included to describe the diffuse density) refined to 0.44(1), which indicates a far greater diffuseness than the 3d radial density function used as the starting value. The κ'' values for the ligating N and O atoms were 0.70(2) and 0.78(2), respectively, again indicating a move toward greater diffuseness. As required for non-centrosymmetric structures, special care was taken to check the absolute values, shifts, and esd's of the odd-order multipoles to ensure that they are well defined in the refinement. In all cases they appeared to have reasonable values and the supposed difficulties specific to non-centrosymmetric systems[34] were not immediately obvious. The typical esd for the multipole parameters, at 0.03, is marginally higher than the average value of 0.02 usually encountered for small organic charge density studies, but given that this is a large transition metal complex, this is not unreasonable. An isotropic extinction parameter (type 1, Gaussian distribution[42]) was also included in the refinement. This "best" refinement has a residual peak

(29) Clementi, E.; Roetti, C. *At. Data Nucl. Data Tables* **1974**, *14*, 177−478.
(30) Kurki-Suonio, K. *Isr. J. Chem.* **1977**, *16*, 115−123.
(31) Stewart, R. F.; Davidson, E. R.; Simpson, W. T. *J. Chem. Phys.* **1965**, *42*, 3175−3187.
(32) Allen, F. H.; Kennard, O.; Watson, D. G.; Brammer, L.; Orpen, A. G.; Taylor, R. *J. Chem. Soc., Perkin Trans. 2* **1987**, Suppl. 1.
(33) Blessing, R. H. *Acta Crystallogr., Sect. B* **1995**, *51*, 816−823.
(34) El Haouzi, A.; Hansen, N. K.; Le Henaff, C.; Protas, J. *Acta Crystallogr., Sect. A* **1996**, *52*, 291−301.
(35) Harel, M.; Hirshfeld, F. L. *Acta Crystallogr., Sect. B* **1975**, *31*, 162−172.
(36) Hirshfeld, F. L. *Acta Crystallogr., Sect. A* **1976**, *32*, 239−244.
(37) Newton, M. D. *J. Chem. Phys.* **1969**, *51*, 3917−3926.
(38) See, for example: Yufit, D. S.; Mallinson, P. R.; Muir, K. W.; Kozhushkov, S. I.; De Meijere, A. *Acta Crystallogr., Sect. B* **1996**, *52*, 668−676. Kampermann, S. P.; Ruble J. R.; Craven, B. M. *Acta Crystallogr., Sect. B* **1994**, *50*, 737−741. Koritsanszky, T.; Buschmann, J.; Luger, P. *J. Phys. Chem.* **1996**, *100*, 10547−10553.
(39) Stevens, E. D.; Coppens, P. *Acta Crystallogr., Sect. A* **1979**, *35*, 536−539.
(40) Holladay, A.; Leung, P.; Coppens, P. *Acta Crystallogr., Sect. A* **1983**, *39*, 377−387.
(41) Stewart, R. F. *J. Chem. Phys.* **1973**, *53*, 1668−1676.
(42) Becker, P. J.; Coppens, P. *Acta Crystallogr., Sect. A* **1974**, *30*, 129−147. *Acta Crystallogr., Sect. A* **1974**, *30*, 148−153. *Acta Crystallogr., Sect. A* **1975**, *31*, 417−425.

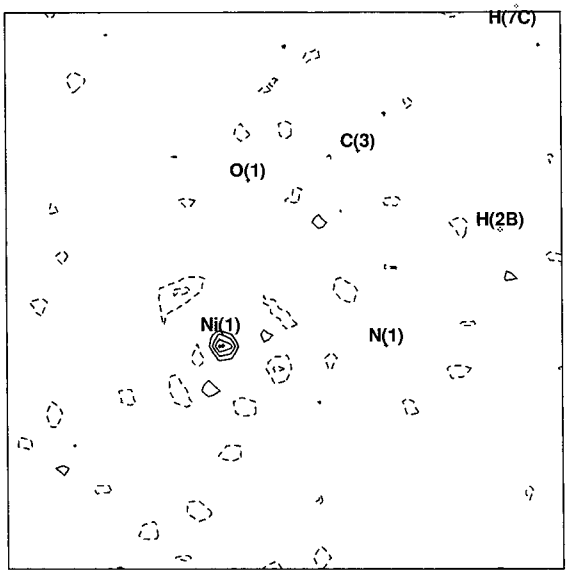

Figure 2. Residual electron density in the N(1), O(1), and Ni(1) plane: contour interval 0.1 e Å^{-3}. Broken lines are negative contours.

of 0.41 e Å^{-3} at the nickel position and other small, unstructured residual features in the nickel coordination sphere as can be seen in Figure 2. Irrespective of the treatment of the metal (including using the neutral scattering factors in place of those corresponding to the doubly charged ion), these residual features could not be further diminished. Additionally, the least-squares correlation coefficients were checked. There were many large ($C_{ij} \geq 0.80$) correlations between multipole parameters describing the density in the $[PF_6]^-$ and $[NO_3]^-$ counterions which are most likely attributable to slight disorder. The only substantial correlations of note in the complex cation were between the off-diagonal components of the ADPs for the nickel, which are constrained by symmetry to be equal, and the single symmetry allowed quadrupole along the 3-fold axis. The correlation coefficient is 0.94, indicating almost complete correlation. One possible explanation for the high correlation is the inadequacy of the Clementi Hartree−Fock scattering factors, which incorporate neither correlation nor relativistic effects. These are probably significant for an element of such a high atomic number.[43]

Given the above-mentioned limitations, slight caution must be applied in the quantitative analysis of the results. However, we assume that the model is qualitatively accurate. The conclusions we draw from these refinements is that the residual maps and *R* factors do not allow one to discriminate between all the models which fit the data reasonably well. It is the physical properties such as the result of the rigid bond test, the appearance of bond paths in the refined model where expected, and the stability and convergence of the refinement which indicate an appropriate model. From our final refinement, it appears necessary to account for the diffuse metal density implicitly and also the metal−ligand overlap density in the model. This we have done by accepting κ'' parameters with more diffuse values than usual on ligating atoms, and a model for the metal atom with greater radial flexibility than normal. Final *R* factors, etc., are incorporated in Table 1, and Figure 2 shows the residual map in the N(1), Ni(1), O(1) plane.

Results

The H_3L Ligand. The results of topological analysis of $\rho(\mathbf{r})$ with respect to the bonding in the ligand is reported in Table 2. As expected for covalent bonds, (3, −1) bond critical points with negative $\nabla^2\rho(\mathbf{r})$ values are observed in all of the intraligand bonds. All C−C bonds have small ellipticities, indicating pure σ bonding, with the values of the electron density at the critical points, ρ_b, in the range 1.80(5)−1.99(4) e Å^{-3}. The C−N bonds show excellent internal agreement and a higher value of ρ_b ranging from 2.06(6) to 2.09(6) e Å^{-3} when compared to the C−C bonds, which correlates well with the observation of the C−N bonds being approximately 0.05 Å shorter. The C−N bonds show slightly higher ellipticities which are likely to be due to polarization at the nitrogen atom end of the bond, rather than any π-contributions to the bonding. Finally, the C−O bond again has bond critical point properties consistent with a polar covalent bond.

Table 2. Critical Point Properties for H_3L

bond	length/Å	ρ_b/e Å^{-3}	$\nabla^2\rho_b$/e Å^{-5}	ϵ
C(1)−C(4)	1.533(1)	1.91(7)	−16.8(1)	0.08
C(2)−C(3)	1.522(1)	1.99(4)	−29.9(1)	0.08
C(3)−C(5)	1.537(1)	1.93(5)	−17.9(1)	0.07
C(5)−C(6)	1.527(2)	1.81(5)	−16.8(1)	0.08
C(5)−C(7)	1.531(2)	1.80(5)	−13.9(1)	0.03
C(1)−N(1)	1.493(1)	2.08(7)	−22.2(2)	0.16
C(2)−N(1)	1.482(1)	2.09(6)	−21.9(2)	0.20
C(4)−N(1)	1.486(1)	2.06(6)	−21.8(1)	0.11
C(3)−O(1)	1.447(1)	1.78(6)	−11.8(3)	0.14

Table 3. Properties at the (3, −3) CPs in $-\nabla^2\rho(\mathbf{r})$ in the VSCC of N(1)

CP	*r*/Å	ρ_c/e Å^{-3}	$\nabla^2\rho(\mathbf{r})_c$/e Å^{-5}
CP(1) → C(1)	0.410	3.6(1)	−72.7(7)
CP(2) → C(2)	0.411	3.6(1)	−66.3(6)
CP(3) → C(4)	0.413	3.6(1)	−65.8(7)
CP(4) → Ni(1)	0.402	4.3(1)	−79.2(6)

Table 4. Angles (deg) between Bond Vectors and Corresponding N(1)−CP Vectors

C(1)−N(1)−CP(1)	6.8	C(4)−N(1)−CP(3)	10.7
C(2)−N(1)−CP(2)	12.3	Ni(1)−N(1)−CP(4)	20.8

Table 5. Properties at the (3, −3) CPs in $-\nabla^2\rho(\mathbf{r})$ in the VSCC of O(1)

CP	*r*/Å	ρ_c/e Å^{-3}	$\nabla^2\rho_c$/e Å^{-5}
CP(5) → C(3)	0.347	6.2(2)	−146(1)
CP(6) → H(O1)	0.344	6.5(2)	−160(1)
CP(7) → Ni(1)	0.345	6.3(1)	−161(1)

One major conclusion of this study is the disposition of the chemical "lone pairs" on the ligating N and O atoms since a conventional picture of the bonding in transition metal complexes predicts a dative bond from the lone pairs to the metal. Unfortunately lone pairs do not reveal themselves in the total density $\rho(\mathbf{r})$. However, it has been observed in a range of molecules that the negative of the Laplacian function of the electronic distribution, $-\nabla^2\rho(\mathbf{r})$, possesses local maxima, or (3, −3) critical points (CPs), in their distributions in every instance where the Lewis electron pair theory requires a lone pair to be present.[20] Additionally there are also (3, −3) CPs in the VSCC in the direction of covalent bonds. Thus an oxygen atom in water exhibits four such features in an approximately tetrahedral arrangement, two which correspond to covalent bonds and two to the lone pairs.[20] In our study, we located four (3, −3) CPs in the VSCC of N(1), three associated with the bonds to carbon and one deriving from the lone pair and contributes to the metal−ligand bond. The angles between the CPs are approximately tetrahedral as expected. Table 3 contains the properties of these CPs, with the nomenclature chosen to indicate the atom toward which the CP is directed. An important observation is that the lone pair which points toward the nickel ion has higher density due to it being a little closer to the nitrogen nucleus. An interesting feature is that the CPs are not directed exactly along the bond vectors. Table 4 shows that the angular deviation of the N(1)−CP vector from the N(1)−X

(43) Wang, J.; Smith, V. H., Jr.; Bunge, C. F.; Jauregui, R. *Acta Crystallogr., Sect. A* **1996**, *52*, 649−658.

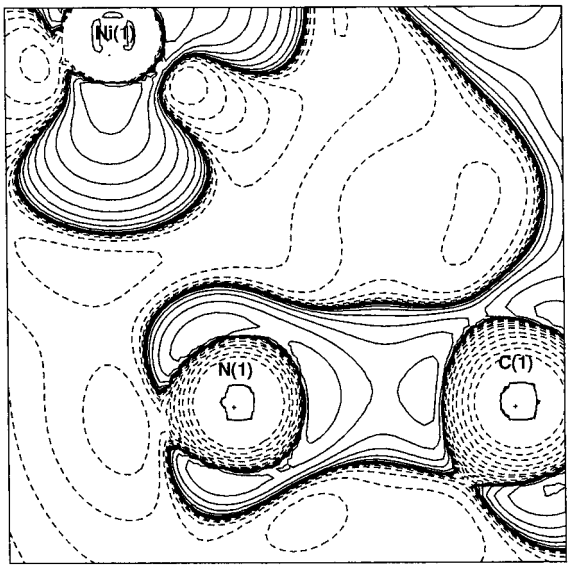

Figure 3. Laplacian distribution in the proximity of N(1); contours at logarithmic intervals in $-\nabla^2\rho$.

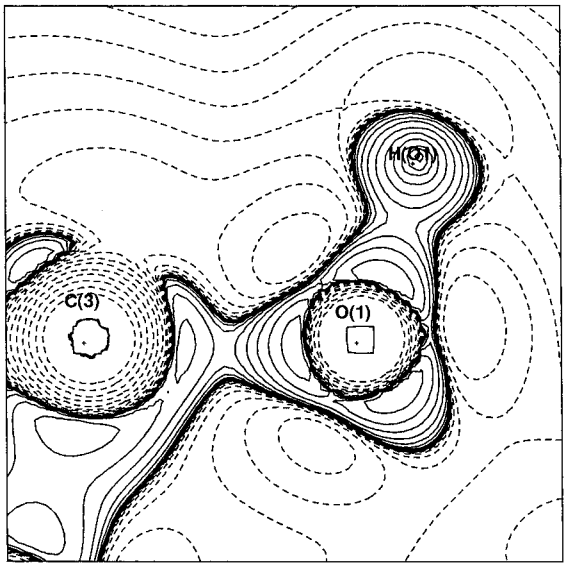

Figure 4. Laplacian distribution in the proximity of O(1).

bond is smallest for the bonds to carbon indicating that these covalent bonds are holding the orientation of the nitrogen atom such that the apex of its tetrahedron, where the lone pair is located, does not point directly at the metal (Figure 3).

The situation for O(1) is a little more complex. If O(1) is sp^3 hybridized as in water or a simple alcohol, we should expect four (3, −3) CPs in a tetrahedral arrangement, corresponding to two bonds and two lone pairs. On complexation with the metal, we may expect one lone pair to act as a σ donor. However if O(1) is sp^2 hybridized, we should see only three (3, −3) CPs arranged in trigonal-planar fashion, two associated with the bonds to C(3) and H(O1) and one acting as a σ-donating lone pair. The remaining unhybridized p-orbital will act as a π-donor to the metal. Our studies show O(1) to possess only three (3, −3) CPs, two for direct, covalent bonds to C(3) and H(O1) and one deriving from the lone pair which contributes to the metal−ligand bond. A mean plane fit of the CPs with O(1) shows them to be almost exactly planar with a maximum deviation of 0.02 Å. The trigonal nature of $-\nabla^2\rho(\mathbf{r})$ about the oxygen atom is shown in Figure 4. This evidence forces the conclusion that O(1) is indeed sp^2 hybridized. However, the three centers to which it is bonded are far from coplanar; the

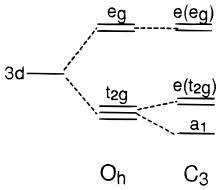

Figure 5. d-orbital energy diagram in O_h and C_3 fields. The ordering of a_1 and $e(t_{2g})$ in C_3 may differ in individual cases.

Table 6. Angular Disposition (deg) of (3, −3) CPs in $-\nabla^2\rho(\mathbf{r})$ in the VSCC of O(1)

C(3)−O(1)−CP(5)	21.8	CP(5)−O(1)−CP(6)	114.6
H(O1)−O(1)−CP(6)	23.3	CP(5)−O(1)−CP(7)	117.9
Ni(1)−O(1)−CP(7)	5.9	CP(6)−O(1)−CP(7)	126.0

angle between the Ni(1)−O(1) vector and the C(3)−O(1)−H(O1) plane is 35.9°. Table 6 shows the orientation chosen by the trigonal planar arrangement of CPs. Since the CP(7)−O(1)−Ni(1) angle is only 5.9°, this proves that, in contrast to the case of the nitrogen atom, the oxygen atom is oriented in the direction which makes the lone pair almost collinear with the bond vector to the metal, rather than maximize the collinearity of the CPs to its directly bonded substituents. The additional consequence of this arrangement is that any π-interaction to the metal from O(1), which must be perpendicular to the plane defined by the three CPs, is maximized.

The Nickel Ion. As with all members of the first period of the transition elements, the charge density distribution of the nickel ion in the bonded environment may be thought of as deriving from 3d density and more diffuse density predominantly of 4s/4p character. The symmetry of the 3d density is gerade and hence can contribute only to the even-order multipoles. Due to the asymmetric coordination geometry of the ligating atoms about the metal atom, the more diffuse metal density associated with metal−ligand overlap will project mainly into a monopolar function and the odd-order multipoles. We included two monopolar functions in the refinement. The first was assigned a 3d radial function while the second monopole shared the κ parameter of 0.44(1) with the odd-order multipoles. Refining the populations of these two monopoles simultaneously is possible in this case due to the large difference in radial extents. The populations obtained of 3d = 7.8(1) and diffuse = 1.3(2) give a net charge of +0.9 for the metal which concurs with chemical expectation, i.e. the formally double charged ion has its charge reduced by donation from the ligands. The values of the populations we have obtained here are remarkably similar to those of Figgis et al.[44] for another Ni(II) complex. They report 3d =7.7(1) and diffuse = 1.61(2) and hence a net charge of +0.8, with a rather different type of refinement.

The total d-orbital charge may be further decomposed[39,40] into symmetry adapted d-orbital populations. For a crystallographically imposed trigonal field, the d-orbital set consists of an a_1 orbital and an e pair, which are a symmetry-adapted derivation from the t_{2g} set in O_h, and a remaining e pair, symmetry adapted from the O_h e_g set. The orbital energy level diagram obtained by relaxing from O_h to C_3 symmetry is shown in Figure 5. The a_1 orbital has the same form as a d_{z^2} orbital oriented along the 3-fold axis, while the $e(t_{2g})$ pair lie perpendicular to this axis in the basal plane. The remaining orbitals are an $e(e_g)$ pair and lie out of the basal plane, with lobes pointing directly at the ligands.

The results of the orbital occupancy determination carried out in this study are displayed in Table 7. They are in the order

(44) Figgis, B. N.; Reynolds, P. A.; Wright, S. *J. Am. Chem. Soc.* **1983**, *105*, 434−440.

Table 7. Symmetry-Adapted d-Orbital Populations

orbital	population	crystal field
a_1	1.60(6)	2.00
$e(t_{2g})$	3.53(7)	4.00
$e(e_g)$	2.62(6)	2.00
$e(t_{2g})e(e_g)$	0.20(13)	

Table 8. Bond Critical Point Properties for the Metal−Ligand Bonds[a]

bond	r_i/Å	r_j/Å	ρ_b/e Å^{-3}	$\nabla^2\rho_b$/e Å^{-5}	ϵ
Ni(1)−N(1)	1.405	0.674	3.10(9)	+1.4(3)	0.15
Ni(1)−O(1)	1.367	0.908	0.93(4)	+9.77(7)	1.29

[a] r_i and r_j are the distances of the bond CP from the first and second atoms respectively.

expected for splitting under a crystal field. However the stabilized a_1 and $e(t_{2g})$ orbitals have lower populations than expected while the destabilized $e(e_g)$ set has a higher population. These facts are consistent with an appreciable ligand-field effect.

The three-dimensional disposition of the diffuse density in the nickel coordination sphere has lobes pointing toward the three ligating nitrogen atoms and a fourth lobe pointing along the 3-fold axis on the oxygen side of the metal and is very diffuse. In form it bears a close similarity to that expected for a set of sp^3 hybrid orbitals composed from a 4s and 4p basis.

Topological Properties of the Metal−Ligand Bonds. Bond paths in $\rho(\mathbf{r})$ for both nitrogen−nickel and oxygen−nickel have been found with the (3, −1) CP properties shown in Table 8. The Ni(1)−N(1) bond CP has a far greater value of the electron density than that for the Ni(1)−O(1) bond. This is due to the observed orientation of the diffuse charge on the metal which orients its lobes directly toward the ligating nitrogen atoms. A second effect of this is the nature of the bond path, which has a total length of 2.10 Å and is therefore almost linear; the direct distance between these atoms is 2.063(1) Å. The bond CP is situated 0.67 Å from the nitrogen terminus. The Ni(1)−O(1) bond path at 2.45 Å is substantially longer than the direct internuclear distance of 2.094(1) Å. Starting at the nickel nucleus, the bond path to oxygen leaves the metal along the diffuse lobe directed along the C_3 axis and then curves around toward the oxygen lone pair, with the bond CP lying 0.91 Å from the oxygen nucleus. For both bonds, the critical point lies much closer to the ligator than to the metal atom reflecting their differing sizes. Interestingly, both critical points show positive Laplacian, which is usually indicative of a closed shell, noncovalent interaction. Given the rather curved nature of the Ni−O bond, the ellipticity is not a particularly reliable indicator of π-bonding and therefore its high value should not be overinterpreted in this context. The ellipticity of the metal−nitrogen bond however is more valuable, since the bond is reasonably linear, and its small value indicates a lack of π-bonding as expected. A plot of $-\nabla^2\rho(\mathbf{r})$ in the plane of N(1), O(1), and Ni(1) is shown in Figure 6. Three-dimensional isosurfaces of $-\nabla^2\rho(\mathbf{r})$ at the −100 and −50 e Å^{-5} levels are shown in Figure 7. These values give the clearest view of the topological properties of $-\nabla^2\rho(\mathbf{r})$ for the oxygen and nitrogen atoms, respectively. It can be clearly seen in three dimensions that the nitrogen lone pair ligates toward a lobe of negative $\nabla^2\rho(\mathbf{r})$ while the single oxygen lone pair ligates between these lobes. Figure 8 shows traces of the bond paths between metal and ligands. Despite there being a total of six ligating atoms, only four bond paths leave the metal. Three conventional, approximately linear bond paths from the metal to the nitrogen atoms are in evidence, while the fourth bond path trifurcates into branches, each leading to an oxygen atom.

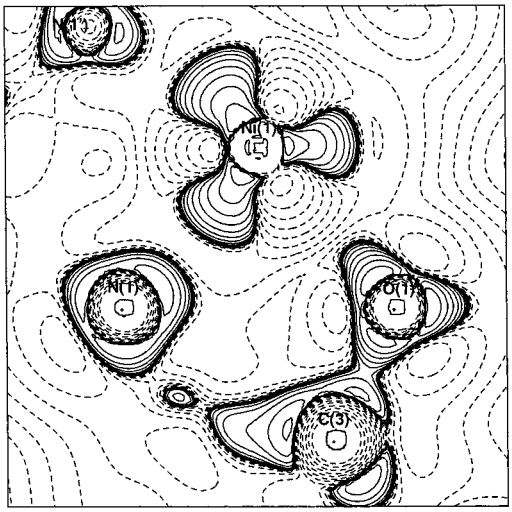

Figure 6. Laplacian distribution in the N(1), O(1), Ni(1) plane.

Discussion

The overall picture of metal−ligand bonding consists of donation of approximately 1.1 electrons to the metal from the ligands as determined by the monopole populations. This donation does not increase the occupancy of the d-orbitals, but does produce an arrangement of diffuse density of approximate tetrahedral symmetry consistent with sp^3 hybridization of the 4s and 4p orbitals. These hybrids point toward the three ligating nitrogen atoms and also along the 3-fold axis between the oxygen atoms. This results in much higher electron density in the Ni−N bonds than the Ni−O bonds. Bond paths in $\rho(\mathbf{r})$ with (3, −1) bond critical points are traceable from metal to ligand. The value of ρ_b in the Ni−N bond is 3.10(9) e Å^{-3}, which is very high and the bond path is almost linear. This contrasts with the Ni−O bond path which follows the diffuse density away from the nickel but then curves toward the oxygen atom (Figure 8). Since the diffuse density on the metal does not point directly at the oxygen atoms, the Ni−O bond has a much lower ρ_b value of 0.93(4) e Å^{-3}. The covalency indicated by the topology of the charge density appears to derive from the diffuse density about the metal rather than preferential occupancy of the individual d-orbitals. The nature of the ligating nitrogen atom is as expected, with a single lone pair pointing at the nickel. The oxygen is sp^2 hybridized with a single lone pair oriented toward the metal atom and an unhybridized p-orbital available for π-bonding.

Both types of metal−ligand bond critical points exhibit positive Laplacian values. In more usual covalent bonds such as C−C, C−N etc., the Laplacian value is negative indicating a local concentration of charge in the bond. In ionic bonds such as Na^+-Cl^- the Laplacian is positive, indicating a local depletion and therefore a closed shell and ionic bond. A literal application of these observations to the less well studied Ni−N and Ni−O bonds would conclude that these bonds are ionic. However, this is at odds with both accepted chemical notions and the other evidence presented here. It has been observed previously that the behavior of the Laplacian becomes less easily interpreted as the diffuseness of the charge density increases. For example, its ability to show shell structure in atoms[45] as local concentrations and depletions of charge no longer holds for $Z \geq 40$. Also, in covalent bonds between electronegative atoms such as in Cl−Cl, $\nabla^2\rho$ has only a small negative value,

(45) Shi, Z.; Boyd, R. J. *J. Chem. Phys.* **1988**, *88*, 4375−4377.

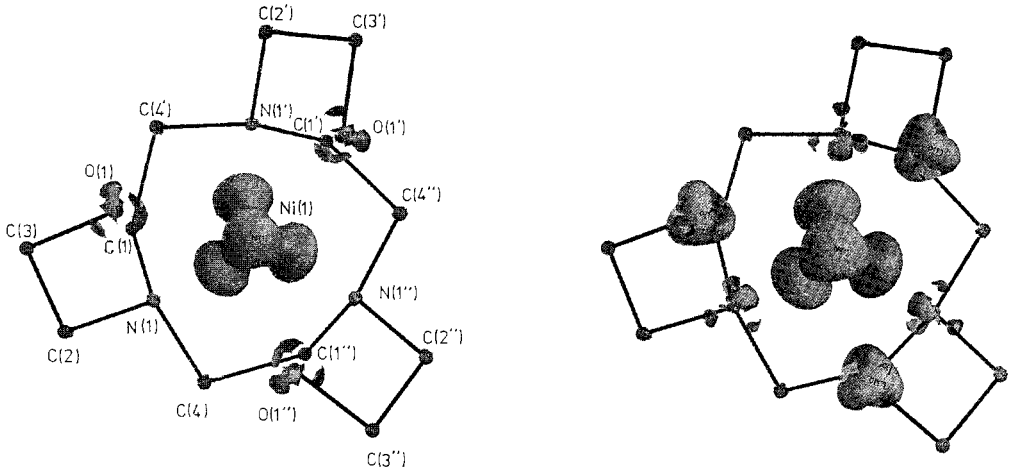

Figure 7. Laplacian isosurfaces in the nickel coordination sphere at the -100 e Å^{-5} (left) and -50 e Å^{-5} (right) levels. The isopropyl substituents have been omitted for clarity. The prime denotes equivalent position *z,x,y*, and double prime denotes equivalent position *y,z,x*.

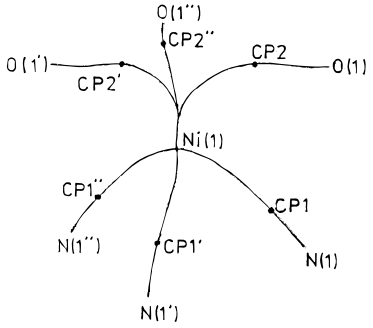

Figure 8. Bond paths for the metal−ligand interactions. Positions of bond critical points are labeled CP(1), etc.

due to the large magnitude of the single positive curvature of the density. In F−F, this curvature is sufficiently large to make $\nabla^2\rho$ positive, even though the bond is obviously covalent.[46] All other published computational studies[47−52] which incorporate Laplacian values in metal ligand bonds also show positive Laplacian and therefore our experimental results provide an important, independent confirmation of this behavior. It would appear that the topological properties of covalent metal−ligand bonding do not have the same characteristics as covalent bonding between first-row atoms.

Conclusion

We have determined the experimental charge density of a large pendant arm macrocyclic complex by fitting a multipole model to high-resolution X-ray diffraction data. We find redistribution of the charge density from the ligating nitrogen and oxygen atoms to the central nickel ion which considerably reduces the charge on the metal. While the metal d-orbital populations are in accord with ligand-field modification of the populations predicted by crystal-field theory, the characteristics of the charge density on the metal are dominated by four diffuse lobes which point at the ligating nitrogen atoms but between the ligating oxygen atoms. The disposition of the lobes is consistent with sp^3 hybrids from the 4s and 4p metal orbitals. The properties of the Ni−N and Ni−O bond critical points differ considerably reflecting the chosen orientation of the diffuse hybrids which is presumably determined by the differing ligating properties of the two atom types. Additionally, the (3, −3) critical points in $-\nabla^2\rho(\mathbf{r})$ within the VSCC of the ligating oxygen atom provide evidence for metal−oxygen π-bonding. We have shown this technique to be tractable for large molecules with many electrons, even when they crystallize in non-centrosymmetric space groups.

Acknowledgment. We thank the EPSRC for support (GR/F 77852, GR/J 22702) and for a postgraduate studentship for G.T.S.

Supporting Information Available: Tables giving fractional atomic coordinates, mean-square atomic displacements, bond lengths and angles, multiple population coefficients, definitions of local axes, and κ values (6 pages). See any current masthead page for ordering and Internet access instructions

JA964264Q

(46) Tsirelson, V. G.; Zou, P. F.; Tang, T.-H.; Bader, R. F. W. *Acta Crystallogr., Sect. A* **1995**, *51*, 143−153.
(47) Maseras, F.; Lledos, A.; Costas, M.; Poblet, J.-M. *Organometallics* **1996**, *15*, 2947−2953.
(48) Bo, C.; Costas, M.; Poblet, J.-M.; Rohmer, M.-M.; Benard, M. *Inorg. Chem.* **1996**, *35*, 3298−3306.
(49) Bo, C.; Saraso, J.-P.; Poblet, J.-M. *J. Phys. Chem.* **1993**, *97*, 6362−6366.
(50) Costas, M.; Bo, C.; Poblet, J.-M. *Chem. Phys. Lett.* **1992**, *200*, 8−14.
(51) Lin, Z. Y.; Hall, M. B. *Inorg. Chem.* **1991**, *30*, 646−651.
(52) Bo, C.; Poblet, J.-M.; Benard, M. *Chem. Phys. Lett.* **1990**, *169*, 89−96.